Technical Notes

Development of an Alternative Delayed Detached-Eddy Simulation Formulation Based on Elliptic Relaxation

Neil Ashton,* Alistair Revell,† Robert Prosser,‡ and Juan Uribe§
University of Manchester, Manchester, England M13 9PL, United Kingdom

DOI: 10.2514/1.J051808

Nomenclature

C_D	=	drag coefficient
C_{DDES}	=	empirical parameter
C_f	=	skin-friction coefficient
C_L	=	lift coefficient
C_p	=	pressure coefficient
$C_{\varepsilon 1}$	=	model constant for the dissipation equation
$C_{\varepsilon 2}$	=	model constant for the dissipation equation
c	=	chord length
f	=	elliptic operator
f_d	=	delayed detached-eddy simulation blending function
h	=	hill height
k	=	turbulent kinetic energy
L	=	turbulent length scale
Re	=	Reynolds number
S	=	deformation tensor
U_b	=	bulk velocity
U_∞	=	freestream velocity
y	=	distance to the nearest wall
y^+	=	nondimensional wall distance
Δ	=	large-eddy simulation filter width
Δt	=	time step
ε	=	turbulent dissipation
κ	=	von Kármán constant
ν	=	molecular viscosity
ν_t	=	turbulent viscosity
Ψ	=	delayed detached-eddy simulation correction term

Introduction

IN RECENT years, hybrid Reynolds-averaged Navier-Stokes (RANS)–large-eddy simulation (LES) models have become a viable compromise between RANS and LES methods for solving massively separated turbulent flows, which frequently occur in aerospace applications. The shortcomings of RANS models and the excessive computational expense of a fully resolved LES have provided a void for these hybrid approaches to fill.

One of the more common hybrid RANS–LES methods in use is the delayed detached-eddy simulation (DDES) approach [1], which is an improved version of the original detached-eddy simulation (DES) method [2]. Both forms are commonly used in the aerospace industry and research alike. DDES can be seen as a three-dimensional unsteady model based on an underlying off-the-shelf RANS model. It seamlessly joins a subgrid-scale model in regions where the numerical grid is fine (and outside of the attached boundary layer) to a RANS model in all other regions.

The principle of DDES is to modify the RANS length scale L_{RANS} as follows:

$$L_{\text{DDES}} = L_{\text{RANS}} - f_d \max(0, L_{\text{RANS}} - L_{\text{LES}}),$$
$$f_d = 1 - \tanh\left[\left(8\frac{\nu_t + \nu}{\sqrt{U_{i,j}U_{i,j}}\kappa^2 y^2}\right)^3\right] \quad (1)$$

in which $L_{\text{LES}} = \Psi C_{\text{DDES}}\Delta$. Ψ is a correction term to ensure the model returns to the classical Smagorinsky form when in LES mode; $f_d \approx 1$ in the LES region and decreases to 0 in the RANS regions. The original DES method was based on the Spalart–Allmaras (SA) [3] model. Since then, several RANS models have been applied to DES and DDES. By far, the most popular models are based on the SA and k-ω shear-stress transport (SST) [4] models.

The issue of model sensitivity within DDES, with particular focus on aerospace flows, has recently been investigated [5]. One conclusion from this research was that for flows in which separation occurs due to the presence of a sharp change in geometry, the solution is only weakly dependent on the underlying RANS model. For flows in which separation occurs through an adverse pressure gradient, some sensitivity to the underlying RANS model is observed. The majority of the RANS models tested in [5] were variants of the SA model; no Reynolds stress models or elliptic-relaxation models were tested. At the time, perceived issues over the numerical stability of these models likely informed this decision.

In a similar approach to DES, Delibra et al. [6] used with some success a hybrid RANS–LES method based upon an elliptic-relaxation RANS model to investigate a wall-bounded pin matrix. Like DES, their method modifies the dissipation term of the turbulent kinetic energy equation to damp the turbulent viscosity and resolve more of the flow.

In the current work, a new DDES model is formulated based on the φ-f model [7], which has previously demonstrated both improved modeling of the near-wall physics and numerical robustness for industrial applications.

The φ-f model is a robust version of the code-friendly $\bar{v}^2 - f$ model developed by Lien and Durbin [8]. In this model, $\bar{v}^2$ is replaced by the dimensionless quantity $\varphi = \bar{v}^2/k$, which results in a more stable model that converges more easily and allows the use of larger time steps compared to the model of Lien and Durbin when used with an uncoupled solver. The model is based on the high-Reynolds-number k-ε model [9], but with modifications to impose the correct behavior near the wall, mainly the correct near-wall scaling of ν_t and the use of the Kolmogorov scaling together with a modified φ-dependent $C_{\varepsilon 1}$ term (denoted $C'_{\varepsilon 1}$).

For the φ-f model, the standard DDES modification is made to the turbulent kinetic energy equation:

$$\frac{\partial k}{\partial t} + \bar{U}_j\frac{\partial k}{\partial x_i} = P_k - \underbrace{\varphi\frac{k^{3/2}}{L_{\text{DDES}}}}_{\text{Modified}} + \frac{\partial}{\partial x_j}\left[\left(\nu + \frac{\nu_t}{\sigma_k}\right)\frac{\partial k}{\partial x_j}\right] \quad (2)$$

Received 21 December 2011; revision received 4 May 2012; accepted for publication 22 July 2012; published online 29 November 2012.

*Postgraduate Student, Modelling and Simulation Centre, School of Mechanical, Aerospace and Civil Engineering.

†Lecturer, Modelling and Simulation Centre, School of Mechanical, Aerospace and Civil Engineering.

‡Senior Lecturer, Modelling and Simulation Centre, School of Mechanical, Aerospace and Civil Engineering.

§Research Fellow, Modelling and Simulation Centre, School of Mechanical, Aerospace and Civil Engineering.

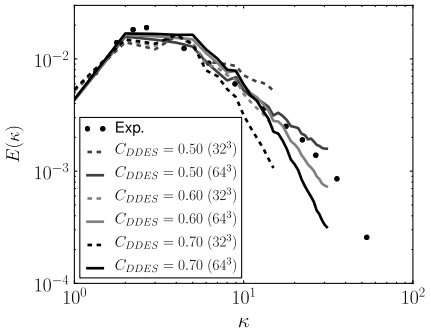

Fig. 1 Calibration of C_{DDES} constant using DIT on 32^3 and 64^3 grids. Exp. denotes experiment.

In the current formulation, the DDES length-scale modification appears only in the turbulent kinetic energy equation and not in the equation for φ. This was chosen to be consistent with the principle of the original DES formulation. Yan et al. [10] investigated the differing results that may be obtained when using an alternative length-scale substitution (through ν_t, which is comparable to also using φ). In the present study, it was decided to establish a baseline version of the φ-f DDES model before investigating alternative substitutions.

Calibration and Validation

The turbulent viscosity should return to a subgrid-scale Smagorinsky-like form when using the DDES length scale $L_{\mathrm{DDES}} = \Psi C_{\mathrm{DDES}}\Delta$ [i.e., $\nu_t = (C\Delta)^2 S$], in which C is a constant. Under local equilibrium conditions (in which production, $P_k = \nu_t S^2$, is equal to dissipation), the k equation (in LES mode) and ε equation become

$$\nu_t S^2 = \frac{\varphi k^{3/2}}{\Psi C_{\mathrm{DDES}}\Delta}, \qquad \nu_t S^2 = \frac{C_{\varepsilon 2}}{C'_{\varepsilon 1}}\varepsilon \tag{3}$$

from which it is straightforward to show that the Smagorinsky form of the φ-f subgrid-scale model is given by

$$\nu_t = A(\Psi C_{\mathrm{DDES}}\Delta)^2 S, \qquad A = \left(\frac{C_{\varepsilon 2}}{C'_{\varepsilon 1}}\right)^{3/2}\left(\frac{1}{\varphi}\right)^{1/2} \tag{4}$$

The correction term Ψ should be of the form $A\Psi^2 = \text{const}$. Unlike the SST–DDES model, A is not a constant and is dependent on φ both directly and via the $C'_{\varepsilon 1}$ parameter. This effectively results in a dynamic φ-dependent LES. The φ dependence is removed by setting

$$\Psi = \left(\frac{C'_{\varepsilon 1}}{C_{\varepsilon 2}}\right)^{3/4}(\varphi)^{1/4} \tag{5}$$

Table 1 Reattachment points for the 2-D periodic hill

Re	Experiment (x/h) [15]	LES (x/h) [14]	SST–DDES (x/h)	φ-f DDES (x/h)
10,590	4.24	4.75	4.26	4.23
37,000	3.76	n/a	4.11	4.10

This cancels out the terms in front of $C_{\mathrm{DDES}}\Delta$ and returns the model to the standard LES mode for DDES.

The C_{DDES} parameter for the new DDES formulation is calibrated using decaying isotropic turbulence (DIT) on two grids consisting of 32^3 and 64^3 cubic and uniform cells. The velocity field is initialized with a suitable instance of isotropic turbulence by the use of an inverse Fourier transform, using the experimental data of Comte-Bellot and Corrsin [11]. To obtain the initial values for other variables, such as the pressure and turbulence quantities, a frozen velocity-field simulation was conducted which, once converged, was used to provide initial conditions for the unsteady turbulence simulation. C_{DDES} is similar to the Smagorinsky constant and must necessarily be calibrated for each DDES formulation. For the φ-f DDES model, a value of $C_{\mathrm{DDES}} = 0.60$ was chosen (Fig. 1).

All calculations were performed using the open-source software Code_Saturne [12,13] developed by EDF R&D. The temporal discretization is second order, while a hybrid numerical scheme based on a blend of central differencing (for the LES zones) and upwinding (for the RANS zones) is used to discretize spatially the convective terms.

This hybrid numerical scheme employs the same f_d function found in DDES and is used to control the numerical scheme as follows:

$$\phi_f = \phi_{f,\mathrm{SOLU}} \quad \text{if } L_{\mathrm{RANS}} < L_{\mathrm{LES}} \tag{6}$$

$$\phi_f = (1 - f_d)\phi_{f,\mathrm{SOLU}} + f_d\phi_{f,\mathrm{CDS}} \quad \text{if } L_{\mathrm{RANS}} > L_{\mathrm{LES}} \tag{7}$$

in which SOLU and CDS represent a second-order upwind-based scheme and a centered scheme, respectively.

Two-Dimensional Periodic Hills

To validate this new DDES formulation, several cases are investigated, the first being the flow over a periodic arrangement of hills whose shape is defined in Fröhlich et al. [14]. The two-dimensional (2-D) computational domain is shown in Fig. 2a, in which h is the hill height and $L_h = 1.93h$, $L_x = 9h$, $L_y = 3.035h$, and the spanwise domain is $L_z = 4.5h$. Flows at two Reynolds numbers were simulated, $Re = 10,590$ and $Re = 37,000$, based on the hill height and the bulk velocity. The case has been investigated extensively because of the strong separation observed after the hill and the complex and rich flowfield, which occurs throughout the domain.

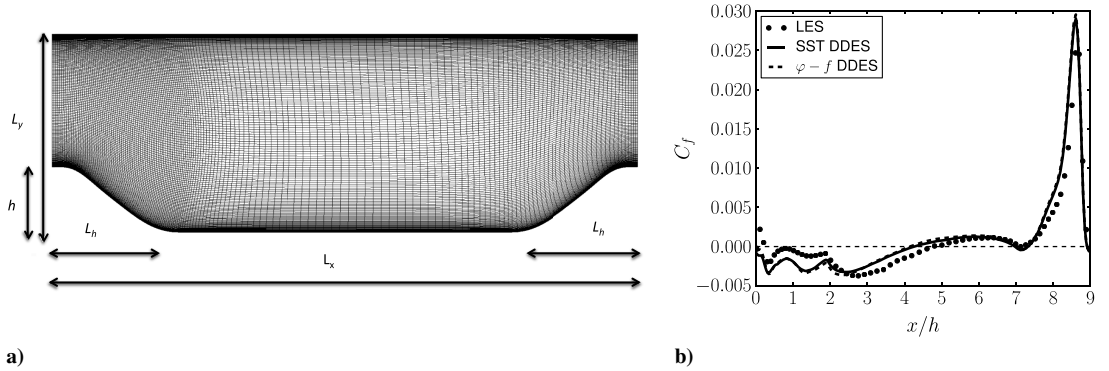

a) b)

Fig. 2 a) Case setup for the 2-D periodic hills, and b) mean spanwise averaged skin-friction coefficient C_f for the two-dimensional periodic hills at $Re = 10,590$.

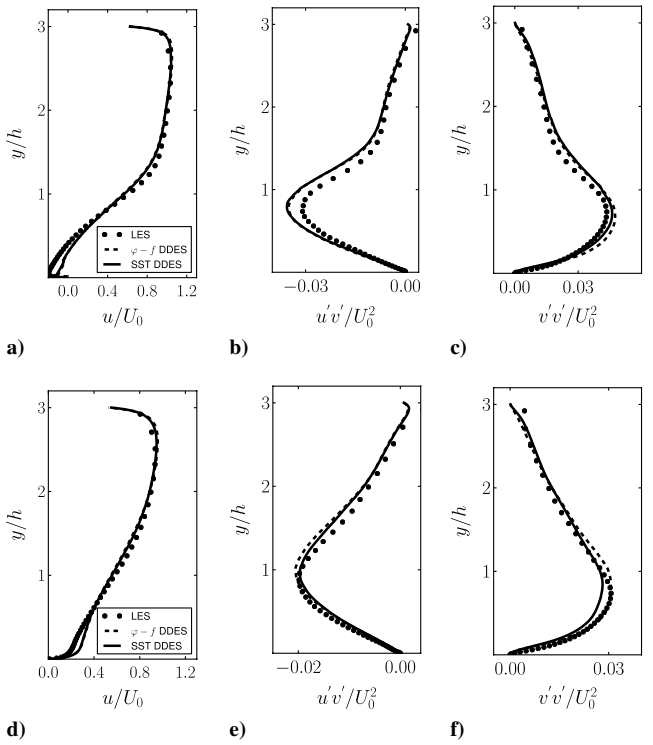

Fig. 3 Mean profiles at $x/h = 3$ for the a) streamwise velocity, b) turbulent shear stress, and c) normal Reynolds, and at $x/h = 6$ for the d) streamwise velocity, e) turbulent shear stress, f) normal Reynolds stress for the 2-D periodic hills.

The mesh ($160 \times 160 \times 60$) is suitably refined near the walls to ensure that $y^+ < 1$. Periodicity is set in the streamwise and spanwise directions, and a no-slip condition is applied to the top and bottom walls. The time step is set to $\Delta t U_b/h = 0.005$ for each simulation, which ensures a $\mathrm{CFL}_{\max} < 1$.

For the majority of the flow, both DDES formulations predict the correct level of turbulent shear stress and, therefore, a similar velocity profile to that of the reference LES [14] and experimental data [15]. There is little variation between the two DDES variants for both Reynolds numbers (Table 1, and Figs. 2b and 3) because both models are in LES mode for the majority of the flow (except the boundary layer). This is not surprising given that this case is known to be fairly insensitive to the underlying model, but nevertheless it serves as a further validation of the new formulation.

NACA 0021 at 60 Deg Incidence

The flow over a symmetric NACA 0021 airfoil at 60 deg angle of attack is also investigated. The flow at this angle of attack is post-stall and exhibits highly unsteady flow features. The Reynolds number is $Re_c = 2.7 \times 10^5$ (based on the chord length c and the freestream velocity U_∞).

An O-type mesh ($140 \times 100 \times 34$) was used, with a time step satisfying $\Delta t U_\infty/c = 0.0025$, again resulting in a $\mathrm{CFL}_{\max} < 1$ in the areas of resolved flow. Each simulation was performed for 1000 convective transit times ($=TU_\infty/c$). Averaging commenced after the initial condition transients had died away (typically 250 transit times). The domain extends a spanwise distance of one chord length and periodicity is applied in this direction.

Table 2 Lift and drag coefficient results from DDES simulations and experimental data for the NACA 0021 airfoil

	Experiment	SST–DDES	φ-f DDES
C_D	1.55	1.75	1.59
C_L	0.93	1.07	0.98
St	0.20	0.18	0.20

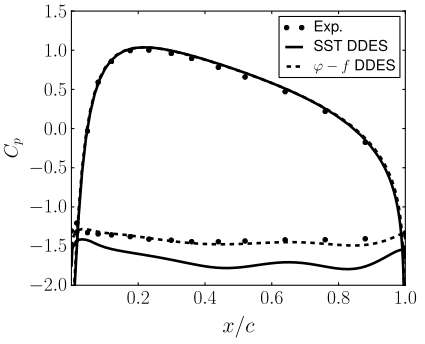

Fig. 4 Mean spanwise averaged pressure coefficient distribution around the NACA 0021 airfoil. Exp. denotes experiment.

Table 2 shows the global force results from both DDES formulations and those provided from the experimental data [16]. The φ-f DDES model matches more closely the experimental data than do the SST–DDES results, as well as predicting a more accurate Strouhal number for the main frequency peak. The improved prediction in pressure distribution (Fig. 4) is clearly manifested in the global lift and drag coefficients. The level of resolved turbulent kinetic energy (TKE) is known to be overpredicted by the SST–DDES model [5], which makes the φ-f DDES model predictions more accurate overall (Figs. 5a and 5b). The level of modeled turbulence is low for both formulations showing that each formulation is in the LES mode (Fig. 6).

The higher level of resolved turbulence for the SST–DDES model means there will be greater fluid mixing in the recirculation zone. This increased mixing brings more higher momentum fluid into the region and reduces the recirculation zone as seen in Fig. 7a. As there is higher momentum in this region compared to that produced by the φ-f DDES model, there results a lower pressure on the upper surface (as seen in Fig. 4) and ultimately higher lift and drag (Table 2).

Figure 8 shows an instantaneous view of the vorticity magnitude for both DDES formulations. For both these models, the resolution of the turbulence is broadly similar, and the structures from the vortex shedding are clear as well as the two shear layers from the leading and trailing edges.

Two-Dimensional Wall-Mounted Hump

The final test case is predominantly characterized by a geometry-induced separation point, and was selected as a challenging case at a recent NASA workshop [17]. The turbulent flow over a wall-mounted 2-D hump (Fig. 9a) at a Reynolds number of $Re_c = 9.36 \times 10^5$ (based on a chord length of $c = 0.42$ m and a freestream velocity of $U_\infty = 34.6$ m/s).

The mesh (Fig. 9b) was provided by New Technologies and Services (NTS) ($379 \times 121 \times 64$) for the Advanced Turbulence Simulation for Aerodynamic Application Challenges (ATAAC) project, and has been found to produce good results for both DDES formulations. A no-slip boundary condition was applied at the bottom wall, and a slip wall was applied to the top wall. Periodic boundary conditions were used in the spanwise direction, which extended a distance of $0.4c$. All cases employed a time step of $\Delta t U_\infty/c = 0.001$, again ensuring $\mathrm{CFL}_{\max} < 1$.

Although the upstream part of the experimental domain was greater than that found in the computation ($-6.39c$ for the former and $-2.14c$ for the latter), work by Šarić et al. [18] shows that there is no significant difference between the choice of the inlet position. The oncoming flow is characterized by a zero-pressure-gradient turbulent boundary layer, whose thickness δ is approximately 57% of the hump height measured at the upstream extent of the domain ($-2.14c$); this corresponds to a momentum-thickness-based Reynolds number $Re_\theta = 7200$ [17]. The mean profiles of the velocity and turbulent quantities used as inlet boundary conditions were taken from a precursor computation; no additional fluctuations were added.

Figure 10 highlights the difference between the two DDES models. The φ-f DDES model predicts the correct recirculation

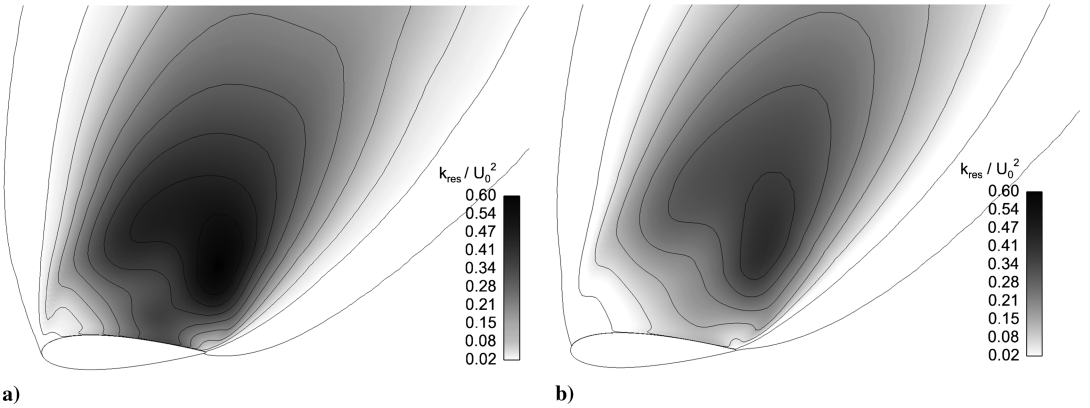

a) b)

Fig. 5 Mean resolved TKE for the a) SST–DDES model and the b) φ-f model for the NACA 0021 airfoil.

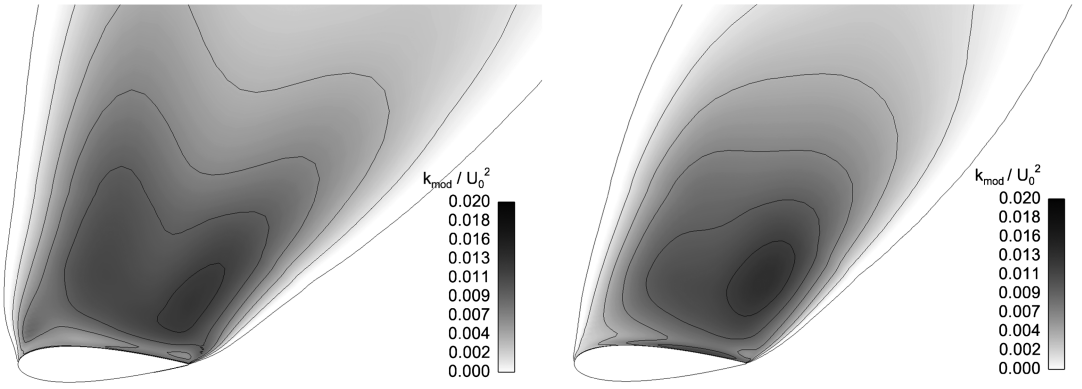

a) b)

Fig. 6 Mean modeled TKE for the a) SST–DDES model and the b) φ-f DDES model for the NACA 0021 airfoil.

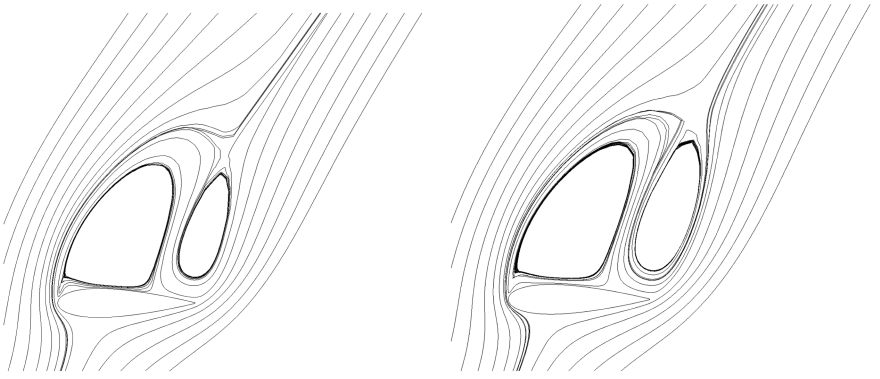

a) b)

Fig. 7 Mean velocity streamlines for the a) SST–DDES model and the b) φ-f DDES model for the NACA 0021 airfoil.

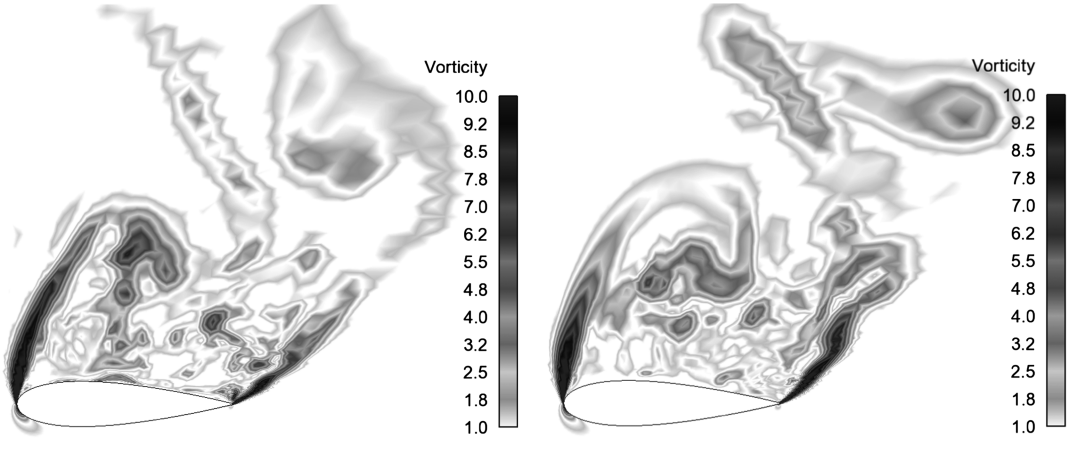

a) b)

Fig. 8 Instantaneous field of vorticity for the a) SST–DDES model and the b) φ-f DDES model for the NACA 0021 airfoil.

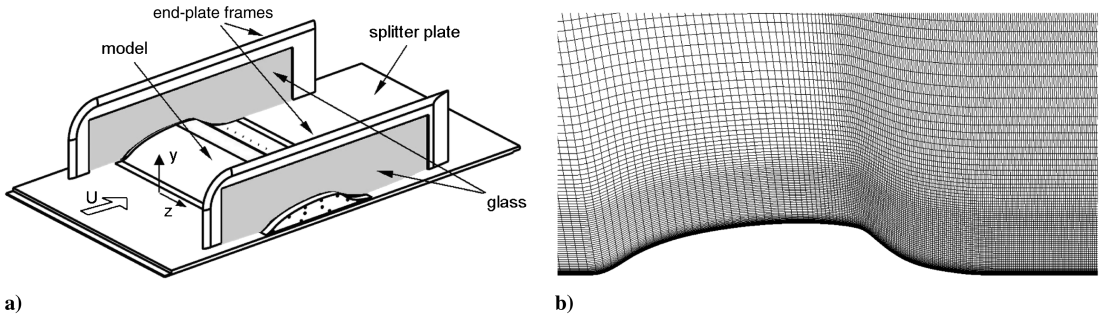

Fig. 9 a) Case setup for the 2-D wall-mounted hump and b) mesh for the 2-D wall-mounted hump.

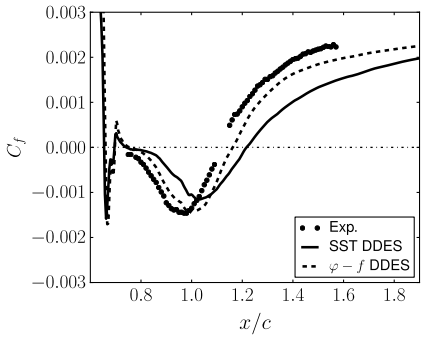

Fig. 10 Skin-friction coefficient for the 2-D wall-mounted hump. Exp. denotes experiment.

strength and matches the experimental reattachment point ($x/c = 1.1$) more closely than the SST–DDES model.

The improved performance of the φ-f DDES model over the SST–DDES model may be attributed to the level of modeled and resolved turbulence levels in the initial part of the recirculation zone ($x/c = 0.66$–0.9). Figure 11 shows the streamwise velocity, shear stress, and normal Reynolds stress for both models at $x/c = 0.9$ and $x/c = 1.0$, in which the improvement shown by the φ-f DDES model is visible. The larger shear-stress values, coupled with larger values for the Reynolds stresses, result in a shorter recirculation region for the φ-f DDES model, which is more consistent with the experimental values.

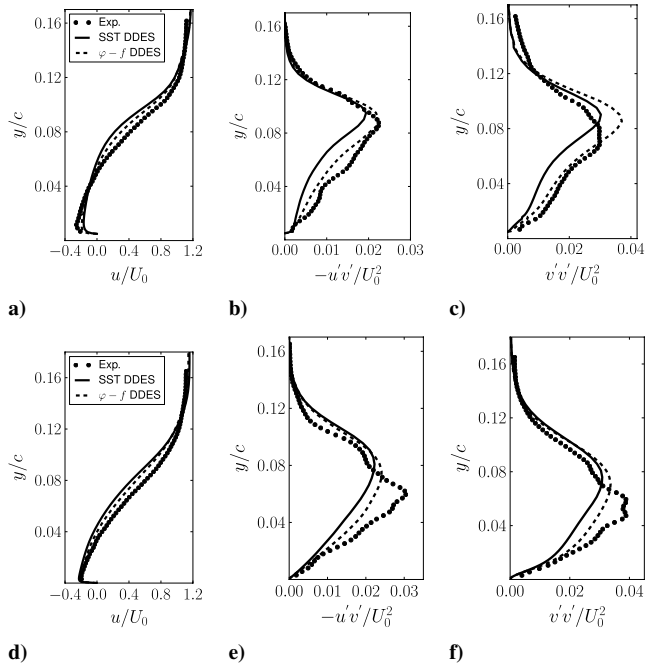

Fig. 11 Mean profiles at $x/c = 0.90$ for the a) streamwise velocity, b) turbulent shear stress, and c) normal Reynolds stress and at $x/c = 1.00$ for the d) streamwise velocity, e) turbulent shear stress, f) normal Reynolds stress for the 2-D wall-mounted hump. Exp. denotes experiment.

The additional transport equation for $\varphi\ (=\bar{v}^2/k)$ enables the model to capture better some of the anisotropy of the flow (by using φ to damp the turbulent viscosity near the wall). It is worth noting that, when observing the predictions of the normal Reynolds stresses, that the error of the experimental particle-image-velocimetry data (for the turbulent quantities) is quoted as being up to 20% [17].

Conclusions

The φ-f delayed detached-eddy simulation (DDES) model has been derived and calibrated using decaying isotropic turbulence (DIT), and then evaluated on three test cases. Suitable formulations of the correction function Ψ and DDES constant C_{DDES} have also been derived and demonstrated using the DIT case. The results from the two-dimensional (2-D) wall-mounted hump and NACA 0021 airfoil are promising and suggest that the underlying Reynolds-averaged Navier–Stokes (RANS) model can play a role in helping to improve future DDES formulations, even for cases with largely fixed separation points. For the 2-D hump, the improved modeling of the near-wall physics improves the prediction of the shear stress, which in turn leads to a better prediction of the strength of the recirculation region. While the φ-f RANS model does involve two further transport equations compared with the shear-stress transport (SST) model, in all cases, the increased computational cost of the φ-f DDES model relative to the SST–DDES model is observed to be low, less than 10% (hump: 9.4%, 2-D hills: 9.7%, NACA 0021: 8.7%).

While the φ-f DDES model is not a fix for the shortcomings of DDES, it is a practical and robust alternative to the established SST–DDES and Spalart–Allmaras–DDES variants that have become the de facto choice for many DDES users.

Acknowledgments

The authors gratefully acknowledge the computational support from the Engineering and Physical Sciences Research Council for the United Kingdom's National High-Performance Computing (HPC) Facility, High End Computing Terascale Resource. Part of this work was carried out under the European Union project Advanced Turbulence Simulation for Aerodynamic Application Challenges (ATAAC) funded by the European Community in the 7th Framework Programme under contract number ACP8-GA-2009-233710-ATAAC. Part of this work was also carried out under the HPC-EUROPA2 project (project number: 228398) with the support of the European Commission–Capacities Area–Research Infrastructures.

References

[1] Spalart, P. R., Deck, S., Shur, M. L., Squires, K. D., Strelets, M. K., and Travin, A., "A New Version of Detached-Eddy Simulation, Resistant to Ambiguous Grid Densities," *Theoretical and Computational Fluid Dynamics*, Vol. 20, No. 3, 2006, pp. 181–195. doi:10.1007/s00162-006-0015-0

[2] Spalart, P. R., Jou, W. H., Strelets, M., and Allmaras, S. R., "Comments on the Feasibility of LES for Wings and on a Hybrid, RANS/LES

Approach," *Advances in DNS/LES, Proceedings of 1st AFOSR International Conference on DNS/LES*, Vol. 1, Greyden Press, Columbus, OH, 1997, pp. 137–147.

[3] Spalart, P. R., and Allmaras, S. R., "A One-Equation Turbulence Model for Aerodynamic Flows," *La Recherche Aérospatiale*, Vol. 1, No. 1, 1994, pp. 5–21.

[4] Menter, F. R., "Two-Equation Eddy-Viscosity Turbulence Models for Engineering Applications," *AIAA Journal*, Vol. 32, No. 8, 1994, pp. 1598–1605. doi:10.2514/3.12149

[5] Haase, W., Braza, M., and Revell, A., (eds.), *DESider — A European Effort on Hybrid RANS–LES Modelling*, Vol. 103, Notes on Numerical Fluid Mechanics and Multidisciplinary Design, Springer–Verlag, Berlin, 2007.

[6] Delibra, G., Hanjalić, K., Borello, D., and Rispoli, F., "Vortex Structures and Heat Transfer in a Wall-Bounded Pin Matrix: LES with a RANS Wall-Treatment," *International Journal of Heat and Fluid Flow*, Vol. 31, No. 5, 2010, pp. 740–753. doi:10.1016/j.ijheatfluidflow.2010.03.004

[7] Laurence, D. L., Uribe, J. C., and Utyuzhinkov, S. V., "A Robust Formulation of the $v^2 - f$ Model," *Flow, Turbulence and Combustion*, Vol. 73, No. 3, 2004, pp. 169–185. doi:10.1007/s10494-005-1974-8

[8] Lien, F. S., and Durbin, P. A., "Non Linear $k - \varepsilon - v^2$ Modelling with Application to High-Lift," *Proceedings of the Summer Program 1996*, Center for Turbulence Research, Stanford Univ., Stanford, CA, 1996, pp. 5–22.

[9] Jones, W. P., and Launder, B. E., "The Prediction of Laminarization with a Two-Equation Model of Turbulence," *International Journal of Heat and Mass Transfer*, Vol. 15, No. 2, 1972, pp. 301–314. doi:10.1016/0017-9310(72)90076-2

[10] Yan, J., Mockett, C., and Thiele, F., "Investigation of Alternative Length Scale Substitutions in Detached-Eddy Simulation," *Flow, Turbulence and Combustion*, Vol. 74, No. 1, 2005, pp. 85–102. doi:10.1007/s10494-005-6916-y

[11] Comte-Bellot, G., and Corrsin, S., "Simple Eulerian Time Correlation of Full and Narrow-Band Signals in Grid-Generated Isotropic Turbulence," *Journal of Fluid Mechanics*, Vol. 48, No. 2, 1971, pp. 273–337. doi:10.1017/S0022112071001599

[12] Archambeau, F., Mechitoua, N., and Sakiz, M., "A Finite Volume Method for the Computation of Turbulent Incompressible Flows—Industrial Applications," *International Journal on Finite Volumes*, Vol. 1, No. 1, 2004, pp. 1–62.

[13] Fournier, Y., Bonelle, J., Moulinec, C., Shang, Z., Sunderland, A., and Uribe, J., "Optimizing Code_Saturne Computations on Petascale Systems," *Computers and Fluids*, Vol. 45, Feb. 2011, pp. 1–6. doi:10.1016/j.compfluid.2011.01.028

[14] Fröhlich, J., Mellen, C. P., Rodi, W., Temmerman, L., and Leschziner, M., "Highly Resolved Large-Eddy Simulation of Separated Flow in a Channel with Streamwise Periodic Constrictions," *Journal of Fluid Mechanics*, Vol. 526, 2005, pp. 19–66. doi:10.1017/S0022112004002812

[15] Rapp, C., and Manhart, M., "Flow Over Periodic Hills: An Experimental Study," *Experiments in Fluids*, Vol. 51, No. 1, 2011, pp. 247–269. doi:10.1007/s00348-011-1045-y

[16] Swalwell, K. E., Sheridan, J., and Melbourne, W. H., "Frequency Analysis of Surface Pressures on an Airfoil After Stall," *AIAA Applied Aerodynamics Conference*, AIAA, Reston, VA, 2003, pp. 1–8.

[17] Greenblatt, D., Paschal, K. B., Yao, C. S., Harris, J., Schaeffler, N. W., and Washburn, A. E., "A Separation Control CFD Validation Test Case, Part 1: Baseline and Steady Suction," AIAA Paper 2004-2220, July 2004.

[18] Šarić, S., Jakirlić, S., Djugum, A., and Tropea, C., "Computational Analysis of Locally Forced Flow Over a Wall-Mounted Hump at High-Re Number," *International Journal of Heat and Fluid Flow*, Vol. 27, No. 4, 2006, pp. 707–720. doi:10.1016/j.ijheatfluidflow.2006.02.015

S. Fu
Associate Editor